SCIENTIFIC REPORTS

OPEN

SUBJECT AREAS:
CHARACTERIZATION AND ANALYTICAL TECHNIQUES
STRUCTURAL PROPERTIES
NANOPARTICLES
TRANSMISSION ELECTRON MICROSCOPY

Received
11 September 2013

Accepted
15 November 2013

Published
4 December 2013

Correspondence and requests for materials should be addressed to D.F.S. (Dario.FERREIRASANCHEZ@cea.fr)

* Current address: LETI/DTSI/SCMC, Commissariat à l'énergie atomique, Grenoble, France.

† Current address: Department of Electronic Materials Engineering, Australian National University, Canberra, Australia.

New approach for structural characterization of planar sets of nanoparticles embedded into a solid matrix

Dario F. Sanchez[1]*, Gabriel Marmitt[1], Cristiane Marin[1], Daniel L. Baptista[1], Gustavo de M. Azevedo[1], Pedro L. Grande[1]† & Paulo F. P. Fichtner[1,2]

[1]Instituto de Física, Universidade Federal do Rio Grande do Sul (IF-UFRGS), Brazil, [2]Department of Metallurgy, Engineering School UFRGS, Brazil.

In this work we demonstrate that Medium Energy Ion Scattering (MEIS) measurements in combination with Transmission Electron Microscopy (TEM) or Grazing Incidence Small Angle X-Ray Scattering (GISAXS) can provide a complete characterization of nanoparticle (NP) systems embedded into dielectric films. This includes the determination of the nanoparticle characteristics (location, size distribution and number concentration) as well as the depth distribution and concentration of the NP atomic components dispersed in the matrix. Our studies are performed considering a model case system consisting of planar arrangements of Au NPs (size range from 1 to 10 nm) containing three distinct Au concentrations embedded in a SiO_2 film.

The physical properties of metallic nanoparticle (NP) systems embedded in dielectric substrates depend not only on the NP parameters (location, size distribution and number concentration) but also on the quality of the dielectric matrix around the NPs. This applies for photonic devices[1] and most particularly for the development of nonvolatile, high areal number density and low power memory devices[2–4]. Degraded dielectrics allow trap-to-trap tunneling processes reducing the charge accumulated in the NPs, while high quality dielectrics improve the memory window, its write/erase speed and its retention and endurance properties[5,6]. The impurity content of a dielectric matrix is a critical degradation issue. The NPs system itself can be regarded as one major source of matrix impurities. The NPs are thermodynamically unstable and lead to the formation of a solute concentration field of their constituent atoms dissolved within the surrounding matrix as provided, for example, by the Gibbs-Thomson effect[7]. For Ge NPs in silica, empirical evidence shows that a significantly high fraction of the total Ge content in the sample (from 20 to 70%) may remain dissolved in the matrix even after high temperature thermal treatments[8–10]. In this case it is argued that, since Ge and Si behave similarly with respect to the formation of tetrahedral bonding structures, Ge atoms could indeed replace Si ones in the SiO_2 lattice and therefore present a high solubility limit. In contrast, for other elements with distinct chemical properties, it is generally expected a rather low solubility limit. However, for NP systems produced under non thermodynamic-equilibrium conditions, solute concentrations are difficult to predict and may achieve sufficiently high values treading the quality of the surrounding dielectric matrix. Hence, it seems worthwhile to develop reliable techniques and methodologies to investigate and characterize NP systems embedded in a solid matrix, not only determining their microstructure properties (size distribution, shape and space arrangement) but also the characteristics of the corresponding solute field.

In the present contribution we demonstrate that Medium Energy Ion Scattering (MEIS) measurements and Rutherford Backscattering Spectrometry (RBS), in combination with pertinent data from Transmission Electron Microscopy (TEM) and/or Grazing Incidence Small Angle X-ray Scattering (GISAXS) can indeed provide a rather complete and accurate characterization of buried NP systems. Our studies are performed considering a model case system consisting of planar arrangements of Au NPs containing three distinct Au concentrations embedded in a SiO_2 film.

GISAXS and TEM are well-established techniques to investigate microstructural properties of such NP systems[11,12]. Only recently, the potential of MEIS as a tool for the characterization of shape, sizes, local composition

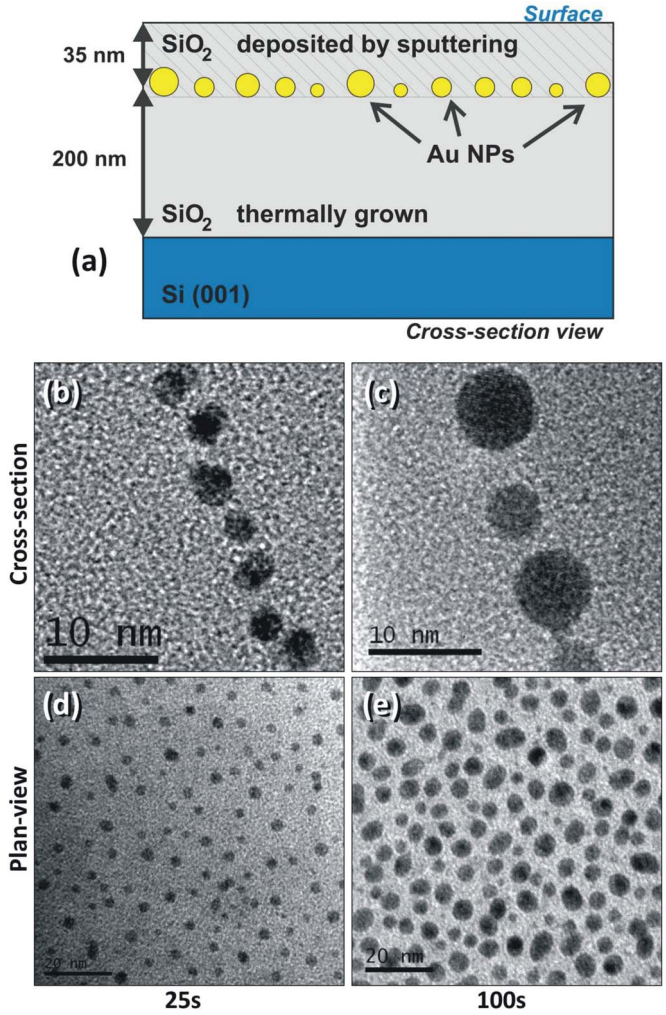

Figure 1 | (a) Schematic cross-sectional illustration of the samples. TEM micrographs present cross-section (b, c) and plan-view (d, e) images of the samples prepared with 25 and 100 s, respectively (diffraction contrast bright field imaging conditions, underfocus).

and stoichiometry of NPs systems has been more systematically explored, but mostly for surface located nanostructures[13–16]. For more complex systems the MEIS potentialities can be significantly enhanced with the aid of simulation codes such as the PowerMEIS[17,18]. This code also accounts for multiple scattering effects, which otherwise tend to blur the information extracted from buried NP systems[19]. In the present contribution we demonstrate that, it is possible to obtain detailed information not only on the microstructure properties of the Au NPs but also on the dissolved part of the Au content (atomically or as small clusters with a few tens of atoms), which was quantified according to their concentration and the depth distribution.

Results

Figure 1a shows a cross-section sketch to illustrate the samples layout. Figures 1b–e presents cross-sectional and plan-view TEM micrographs obtained from samples deposited during 25 and 100 s. Planar sets of Au NPs, apparently of the Volmer–Weber type[20], are observed for all cases including the 50 s deposited sample (not shown). The plan view micrographs directly allows the determination of the NPs areal densities corresponding to: $(13 \pm 1) \times 10^{11}$ NP cm^{-2} for the 25 s deposition case, $(11 \pm 1) \times 10^{11}$ NPs cm^{-2} for the 50 s case and $(15.3 \pm 0.5) \times 10^{11}$ NPs cm^{-2} for the 100 s case.

Figure 2 shows the size distribution of the NPs as obtained by TEM observations and GISAXS measurements. For 25 and 50 s, the particles are quite spherical-like and their size evaluation is straightforward. For the 100 s case, the particles are rather oblate. Hence, accurate characteristic sizes could not be directly deduced from the GISAXS measurements. From the TEM micrographs, however, they were estimated by the average from the largest and smaller diameters. We notice that the results from the TEM observations present larger mean sizes and variances as compared to the corresponding ones evaluated from the GIXAXS measurements. These differences may be attributed to the distinct sampling conditions from each technique. For TEM, typically about 300 particles were counted from a very small region of the sample while GISAXS probes a sample area about 10^8 times higher. In addition, to enhance the contrast, TEM images of small particles are usually taken in out-of-focus conditions which tend to artificially enlarge the particle sizes[21].

The total amount of the deposited Au measured by MEIS (and confirmed by RBS measurements) for the 25, 50 and 100 s samples are 1.8, 3.1 and 7.4×10^{15} Au atoms/cm^2, respectively. Taking into account the total amount of deposited Au, MEIS simulations were carried out using the PowerMEIS code[22]. An analysis without considering the TEM data could lead to unrealistic results since there are many free parameters in the simulation. Therefore the NP sizes and number concentration obtained by TEM were used as an input to the simulations[18]. In order to simulate a MEIS spectrum one has to assume a particular geometrical shape, atomic composition and density. In the present case we assumed 2D arrays of spherical NPs with given radius and areal density. Since the total amount of atoms is fixed, only the NP radius was adjusted.

The simulated spectra are then compared with the measured ones as illustrated in Figure 3. This figure shows the ion scattering intensity maps as a function of ions scattering angle and energy for the three measured samples. The columns representing the measured and calculated spectra are labeled "experimental" and "simulation". Best fits are determined by the minimum of the reliability function R^2 that reads

$$R^2 = \frac{1}{N}\sum_{i=1}^{N}\left(I_{Sim,i} - I_{Exp,i}\right)^2. \qquad (1)$$

Here, I_{Sim} and I_{Exp} correspond to the simulated and measured ion scattering intensities for scattered angles ranging from 108° to 132° and for scattered energies ranging from 105 to 127 keV. The angle and energy ranges were chosen in order to cover exclusively the Au signal. The calculated spectra in Figure 3 correspond to the best fit obtained by the R^2 criteria.

Figures 4a to 4c show how the reliability function R^2 varies with the NPs radius. The full circles correspond to simulations and the lines are parabolic fittings. The best fit is given by the minimum of the reliability function. The corresponding radius and their uncertainties are indicated in each plot.

Figure 4d shows a comparison of radius determined by the parabolic fit obtained from the MEIS analysis assuming that all Au atoms are contained in the NPs and the NPs size distributions provided by TEM and GISAXS. For the 25 and 50 s cases, the TEM and GISAXS results are consistent with each other and significantly disagree with the results from the MEIS analysis. Unlike GISAXS and TEM, the MEIS probe is sensitive to all Au atoms, regardless if they are contained in NPs or dispersed in the matrix. Hence, for a number density of NPs consistent with the one determined from the plan-view TEM micrographs (see Figure 1), this disagreement indicates that part of the deposited Au content is indeed not contained in TEM or GISAXS detectable NPs, but rather dissolved in the matrix.

In addition, by taking into account the NPs' size distributions of the samples from GISAXS analysis (Figure 2d and 2e), the total amount of Au detected by MEIS and RBS and the NPs number densities from plan-view TEM observations, we can state that only

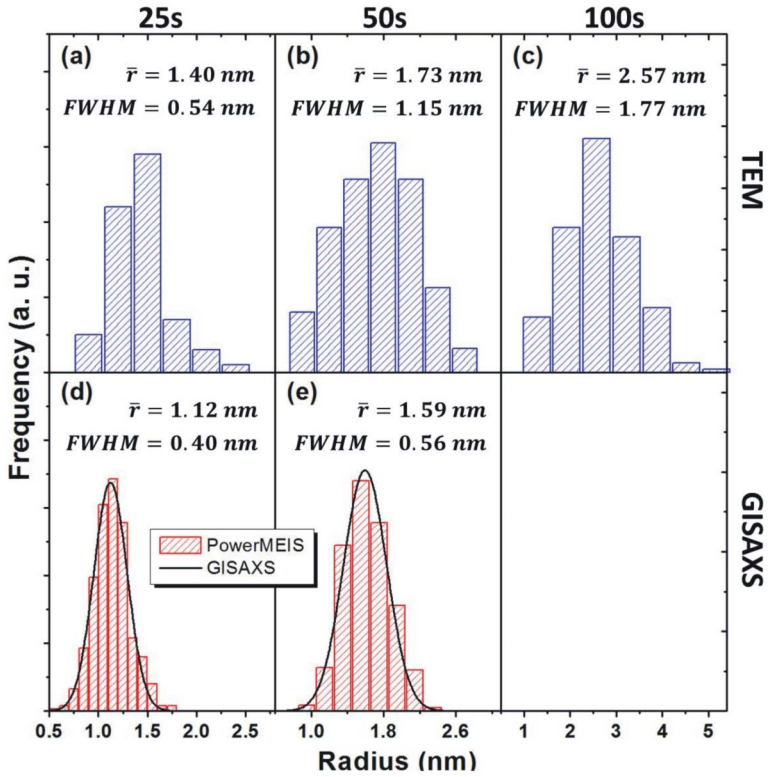

Figure 2 | Particle Size Distributions obtained by TEM (a–c) and GISAXS (d–e) measurements. The corresponding mean radius $\bar{r}$ and FWHM are also indicated.

a small amount of the Au atoms (28 ± 5% for the 25 s sample and 39 ± 9% for the 50 s sample) is actually contained in the NPs. These results are summarized on Table 1. The table also includes the results obtained for the 100 s deposited sample, evaluated considering the size distribution from TEM measurements. For this case we notice that the NPs' mean size obtained by MEIS analysis is slightly larger than the one by TEM, with overlapping uncertainty bars.

The large differences between GISAXS and TEM as compared to the MEIS results can be attributed to the fact that the samples were prepared in conditions away from the thermodynamic equilibrium and therefore a significant fraction of Au atoms have not been incorporated into the particles during the deposition process[23]. Furthermore, during the deposition of the SiO_2 cap layer, it is also possible that additional Au atoms may be re-dispersed from the particles into the silica over layer.

Figure 5 shows TEM micrographs presenting high-resolution annular dark field Z-contrast images from selected particles and their surroundings. The white areas represent the accumulation of Au atoms, which can be detected not only in the NPs but also distributed in the silica matrix surrounding the NPs. These observations are not quantitative but provide a direct evidence of the presence of dispersed Au atoms and subnanometric clusters as suggested by the MEIS measurements.

Discussion

Hence, in order to refine the system characterization, additional MEIS simulations were then performed accounting for the dissolved Au content for the 25 and 50 s sample cases. The basic idea of the simulation concept is illustrated in Figure 5a. It introduces a matrix layer with thickness h and composition $(SiO_2)_xAu_{1-x}$, between the thermally grown and the deposited SiO_2. Figure 6b to 6g shows the corresponding MEIS simulations compared to the experimental scattered intensity profiles for three different scattered angles (109°, 120° and 131°). Two different simulations were performed: 1) with (dashed blue line) and 2) without (continuous red line) the

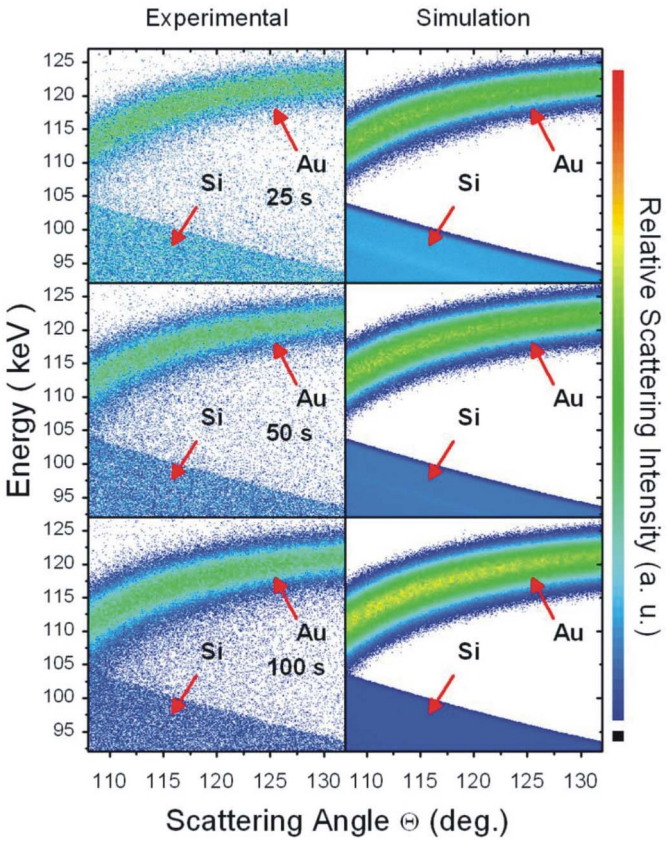

Figure 3 | Experimental and simulated two-dimensional map of ion scattering intensities (2D-MEIS spectra) for the 25, 50 and 100 s deposited samples taken with 150 keV He^+ ions.

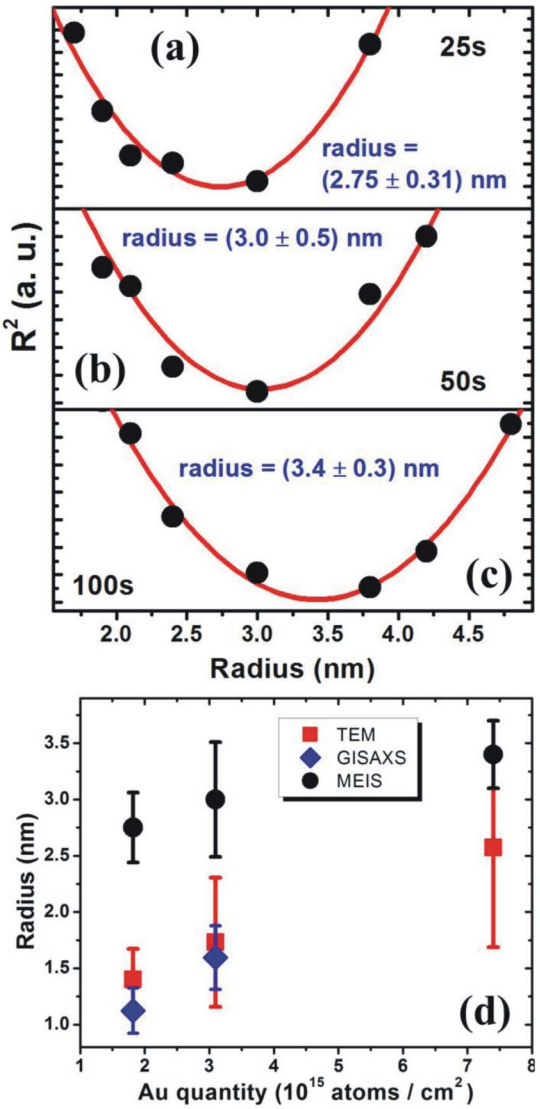

Figure 4 | (a–c) Values of the reliability factor R^2 (black dots) for each sample as a function of the radius of the NPs as deduced from the MEIS analysis. The red lines are eye-guiding curves. (d) Results for the radius of the NPs obtained by TEM, GISAXS and MEIS measurements as a function of the amount of deposited Au.

inclusion of the dissolved part of Au. This comparison highlights the lack of Au when only the NPs are taking into account.

Since the surrounding layer contains the missing gold detected by MEIS and RBS, the thinner layers have larger Au concentrations, as indicated in the x-axis in Figure 7, from where the best fitting was obtained by minimizing the reliability factor R^2 in the same way as done before. The results are shown in Table 2. This procedures show that the combination of TEM and/or GISAXS results with MEIS

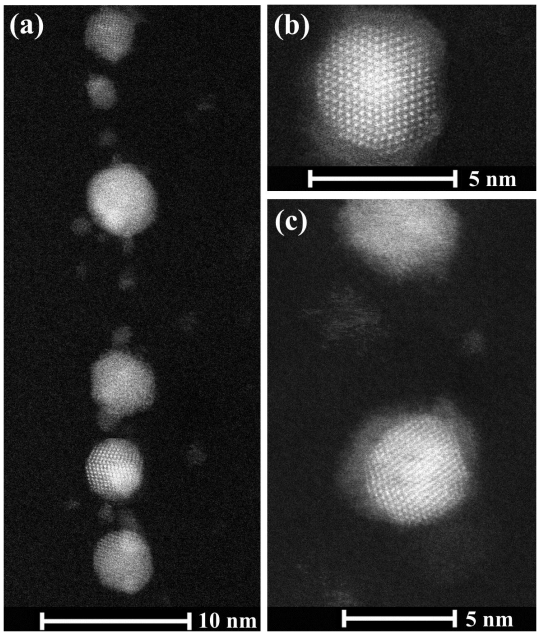

Figure 5 | **High-resolution Z-contrast TEM images acquired through scanning transmission electron microscopy using a high-angle annular dark-field detector.** The images show the nanoparticles and the dispersed Au content within the surrounding matrix.

measurements may provide a consistent description of the system microstructure accounting for the NPs and the dispersed atoms in the matrix. It also tackles a refined way to investigate atomic processes of nanoparticle growth under non-thermodynamic equilibrium conditions.

In this work we investigated three planar sets of buried Au NPs embedded into SiO_2 matrix synthesized with different sputtering deposition times. We observed that, for the samples prepared with 25 and 50 s, a significant fraction of the total amount of Au atoms becomes dissolved within the dielectric matrix around the NPs. Combining MEIS, RBS, TEM and GISAXS measurements, we were able to quantify the fraction of Au atoms effectively contained in the NPs, as well as the concentration and depth distribution of the complementary Au amount dispersed in the matrix around the NPs. These results open new perspectives for a more complete characterization of embedded metallic NPs systems into a solid matrix and the improvement NP bases devices.

Methods

Au atoms were deposited onto 200 nm thick SiO_2 films, thermally grown from (001) Si wafers. The deposition was performed by RF magnetron sputtering, in a pure Ar plasma and with an RF power of 20 W, using an AJA magnetron sputtering device (ATC Orion-8 UHV from NANOLAB, Institute of Physics - UFRGS). A set of three samples containing different amounts of Au were obtained considering deposition times of 25, 50 and 100 s. Without breaking the vacuum, immediately after the Au deposition the samples were covered with a 35 nm thick layer of SiO_2, deposited using similar conditions but with an RF power of 90 W for 67 min.

Table 1 | NP areal number densities and percentage of the total amount of Au present as NPs, taking into account the size distribution from TEM or GISAXS

Sample	NPs areal number density (NPs/cm^2)	Size distribution	Au present as NPs (%)
25 s	(13 ± 1) 10^{11}	GISAXS	28 ± 5
		TEM	59 ± 5
50 s	(11 ± 1) 10^{11}	GISAXS	39 ± 9
		TEM	53 ± 9
100 s	(15.3 ± 0.5) 10^{11}	TEM	112 ± 7

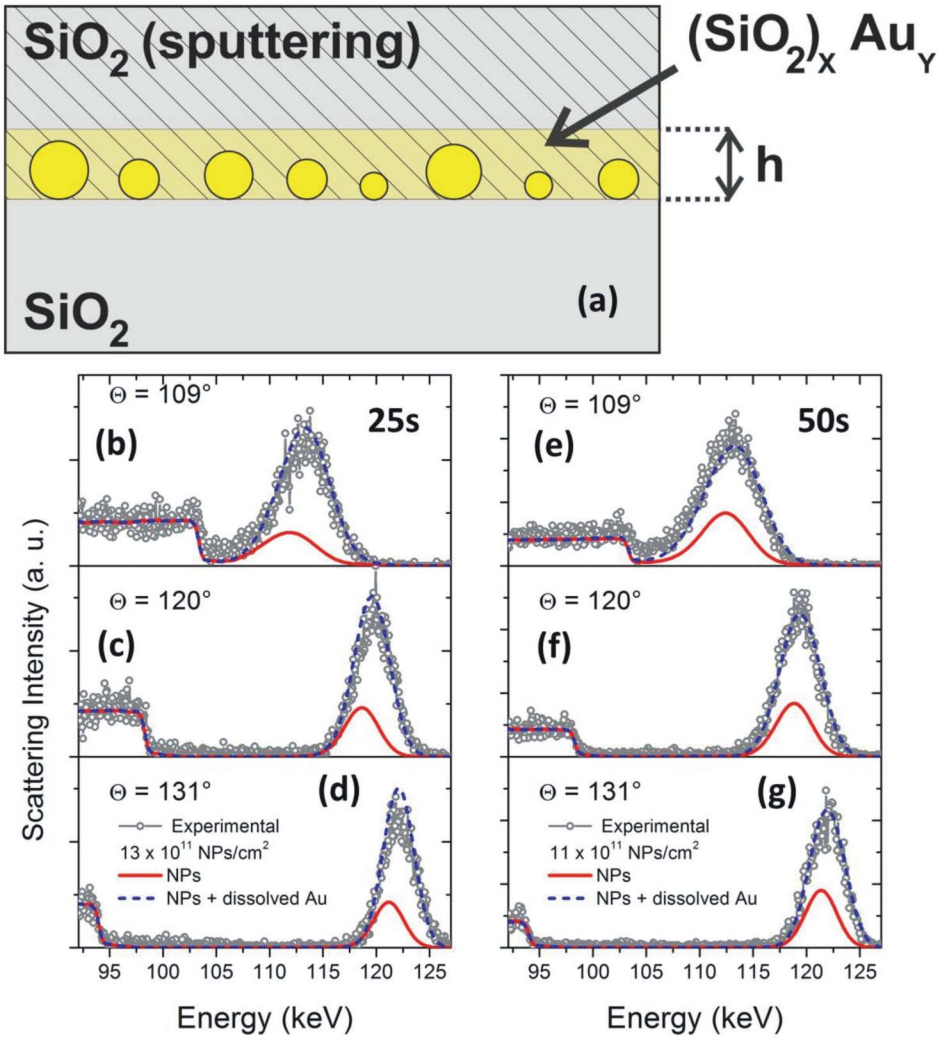

Figure 6 | (a) Illustration of the system characteristics considering the planar set of NPs embedded in a matrix containing Au atoms (i.e. $(SiO_2)_xAu_y$) distributed in a layer with thickness h. (b–g) Results for the 25 and 50 s cases showing the experimental scattered intensities profiles (gray line-circles) as a function of energy for three scattered angles ⊖ and the simulated ones. The simulations considering the Au content present only in the NPs are shown in continuous red lines. Those considering the NPs and the dissolved Au atoms within the surrounding matrix are represented by dashed blue lines.

These samples were then directly investigated by MEIS, RBS, TEM and GISAXS. The MEIS measurements were performed using a 150 keV He^+ ion beam. The samples were mounted in a 3-axis goniometer inside the analysis chamber kept under a pressure of about 10^{-7} mbar. Typical beam current was less than 15 nA. The angle of incidence used was of 10° and backscattered He^+ ions emerging from the target were analyzed using a Toroidal Electrostatic Analyzer (TEA) mounted at 120 degrees with respect to the beam direction. At the top end of the TEA a set of two micro-channel plates coupled to a position-sensitive detector allows each ion to be energy- and angle-analyzed leading to 2-D spectra. The TEA angular aperture is 24 degrees and each angle bin corresponds to 0.08 degrees. The overall energy resolution of the system is 600 eV. Details of the data analysis are described in refs. 17–19, 22. The MEIS analysis was performed using the 500 kV electrostatic accelerator from the Ion Implantation Laboratory (LII), IF–UFRGS. The MEIS measurements were analyzed using the PowerMEIS package[22] where the sample is discretized layer by layer using full 3D matrices. Each one represents a layer, and each element of the matrix stands for specific composition, stoichiometry and density of the material. In this way the set of NPs was generated with specific shapes, size and pair correlation function. The PowerMEIS program can handle any geometric shape, size distribution, and density of the nanostructures. It also accounts for the asymmetry of the energy loss-distribution due to the backscattering collision and to multiple scattering effects.

Standard Rutherford backscattering Spectrometry (RBS) experiments were also performed using a 1.4 MeV He^{2+} ion beam from the 3 MV tandetrom accelerator from the LII-IF-UFRGS.

TEM observations were performed in cross-sectional and plan-view samples prepared by ion milling. The samples were characterized at 200 keV via selected area diffraction measurements (SAD) as well as via diffraction and phase contrast observations modes to determine shape, size, size distribution, spatial order and phase of the NPs using a JEM 2010 microscope from the Center of Electron Microscopy UFRGS. Additional high-resolution observations were carried out in a Cs-corrected FEI Titan 80/300 microscope from the Brazilian National Institute of Metrology (INMETRO). Z-contrast images were acquired through scanning transmission electron microscopy (STEM) using a high-angle annular dark-field detector

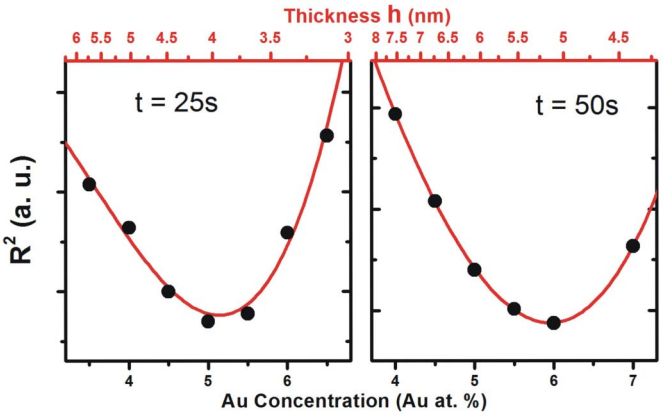

Figure 7 | **The reliability R2 values (black dots) as a function of the Au concentration in the surrounding layer $(SiO_2)_xAu_y$, as illustrated in Figure 5.** The red lines are eye-guiding curves.

Table 2 | The surrounding layer thickness h and the corresponding Au concentration, both obtained from the minimum value of R^2 from Figure 7

Sample	Surrounding layer thickness h (nm)	Au concentration (at.%)
25 s	4.0 ± 0.3	5.1 ± 0.4
50 s	5.1 ± 0.7	6.0 ± 0.9

(HAADF). The GISAXS measurements were performed in the Brazilian Synchrotron Light Source LNLS, with 8.5 keV of X-ray energy. The GISAXS data were analyzed with the FitGISAXS package[24] developed within the IGOR Pro analysis software (WaveMetrics, Inc.).

1. Okubo, N., Umeda, N., Takeda, Y. & Kishimoto, N. Enhancement of metal-nanoparticle precipitation by co-irradiation of high-energy heavy ions and laser in silica glass. *Nucl. Instr. and Meth. B* **206**, 610–614 (2003).
2. Tiwari, S. *et al*. Volatile and non-volatile memories in silicon with nano-crystal storage. Paper presented at Electron Devices Meeting, Washington, DC. Place of publication: IEEE Int. Electron. Devices Meet. Tech. Dig., 521–524 (1995, December).
3. Tiwari, S. *et al*. A silicon nanocrystals based memory. *Appl. Phys. Lett.* **68**, 1377 (1996).
4. Diaz, R., Grisolia, J., Pecassou, B., Shalchian, M. & BenAssayag, G. Functional nanocrystal-based memories with extraction of nanocrystals properties by charge pumping technique. *Solid-State Electron.* **82**, 11–15 (2013).
5. Chen, W. R. *et al*. Formation of stacked Ni silicide nanocrystals for nonvolatile memory application. *Appl. Phys. Lett.* **90**, 112108 (2007).
6. Chen, S.-C. *et al*. Nonvolatile memory effect of tungsten nanocrystals under oxygen plasma treatments. *Thin Solid Films* **518**, 7339–7342 (2010).
7. Porter, D. & Easterling, K. E. *Phase transformations in metals and alloys* (Chapman & Hall, London, 1992).
8. Lopes, J. M. J. *et al*. Cluster coarsening and luminescence emission intensity of Ge nanoclusters in SiO_2 layers. *J. Appl. Phys.* **94**, 6059 (2003).
9. Sahoo, P. K., Gasiorek, S. & Lieb, K. P. Cathodoluminescence and epitaxy after sequential Rb- and Ge-ion implantation in α-quartz. *Nucl. Instr. and Meth. in Phys. Res. B* **240**, 188–193 (2005).
10. Gasperini, A. *et al*. Investigation of indirect structural and chemical parameters of GeSi nanoparticles in a silica matrix by combined synchrotron radiation techniques. *J. Appl. Cryst.* **45**, 71–84 (2012).
11. Renaud, G., Lazzari, R. & Leroy, F. Probing surface and interface morphology with grazing incidence small angle X-ray scattering. *Surf. Sci. Rep.* **64**, 255–380 (2009).
12. Biasiol, G. & Heun, S. Compositional mapping of semiconductor quantum dots and rings. *Phys. Rep.* **500**, 117–173 (2011).
13. Konomi, I., Hyodo, S. & Motohiro, T. Simulation of MEIS spectra for quantitative understanding of average size, composition, and size distribution of Pt–Rh alloy nanoparticles. *J. Catal.* **192**, 11 (2000).
14. Okazawa, T., Kohyama, M. & Kido, Y. Electronic properties of Au nanoparticles supported on stoichiometric and reduced TiO_2(110) substrates. *Surf. Sci.* **600**, 4430 (2006).
15. Quinn, P. D. *et al*. Composition profiles of InAs–GaAs quantum dots determined by medium-energy ion scattering. *Appl. Phys. Lett.* **87**, 153110 (2005).
16. Matsumoto, H. *et al*. Au(core)/Pd(shell) structures analyzed by high-resolution medium energy ion scattering. *Nucl. Instrum. Methods Phys. Res. Sect. B* **268**, 2281 (2010).
17. Sortica, M. A. *et al*. Structural characterization of CdSe/ZnS quantum dots using medium energy ion scattering. *Appl. Phys. Lett.* **101**, 023110 (2012).
18. Leveneur, J. *et al*. Iron-based bimagnetic core/shell nanostructures in SiO_2: a TEM, MEIS, and energy-resolved XPS analysis. *J. Nanopart. Res.* **14**, 1149 (2012).
19. Sanchez, D. F. *et al*. Structural characterization of Pb nanoislands in SiO_2/Si interface synthesized by ion implantation through MEIS analysis. *Surf. Sci.* **605**, 654–658 (2011).
20. Ruffino, F., Giannazzo, F., Roccaforte, F., Raineri, V. & Grimaldi, M. G. *Toward Functional Nanomaterials* [Wang, Z. M. (ed.)] [127–171] (Springer, New York, 2009).
21. Jenkins, M. L. & Kirk, M. A. *Characterization of Radiation Damage by Transmission Electron Microscopy,* (IOP Publishing Ltd, London, 2001).
22. Sortica, M. A., Grande, P. L., Machado, G. & Miotti, L. Characterization of nanoparticles through medium-energy ion scattering. *J. Appl. Phys.* **106**, 114320 (2009).
23. Ruffino, F. *et al*. Self-organization of gold nanoclusters on hexagonal SiC and SiO_2 surfaces. *J. Appl. Phys.* **101**, 064306 (2007).
24. Babonneau, D. FitGISAXS: software package for modelling and analysis of GISAXS data using IGOR Pro. *J. Appl. Cryst.* **43**, 929–936 (2010).

Acknowledgments

The authors acknowledge the financial support by brazilian agencies CNPq, FAPERGS, PRONEX program, the use of the infrastructure of Center for Electron Microscopy and the Ion Beam Implantation Laboratory at UFRGS and of the facilities from the Brazilian National Institute of Metrology and the Brazilian Synchrotron Light Laboratory (XRD2 beam line).

Author contributions

G.M. worked on the modification of the PowerMEIS source code by including Multiple Scattering effects, which is important for buried nanostructures in solid matrix. C.M. worked on the sample synthesis and GISAXS experiments. D.L.B. measured and analyzed by STEM-HAADF and prepared the figure 6. G.M.A. worked on the GISAXS experiments and analysis. P.L.G. worked on the MEIS experiments and analysis. P.F.P.F. worked on the TEM experiments and analysis. D.F.S. wrote the main manuscript text, prepared the figures, planed and worked on the MEIS, GISAXS and TEM experiments and analysis, planed and worked on the sample synthesis and prepared all the samples for TEM and STEM-HAADF experiments. All authors reviewed the manuscript.

Additional information

Competing financial interests: The authors declare no competing financial interests.

How to cite this article: Sanchez, D.F. *et al*. New approach for structural characterization of planar sets of nanoparticles embedded into a solid matrix. *Sci. Rep.* **3**, 3414; DOI:10.1038/srep03414 (2013).